THE ASTRONOMICAL JOURNAL, 115:1680–1687, 1998 April

A SEMIAUTOMATED SKY SURVEY FOR SLOW-MOVING OBJECTS SUITABLE FOR A PLUTO EXPRESS MISSION ENCOUNTER

CHADWICK TRUJILLO AND DAVID JEWITT
Institute for Astronomy, University of Hawaii, 2680 Woodlawn Drive, Honolulu, HI 96822;
chad@ifa.hawaii.edu, jewitt@ifa.hawaii.edu
Received 1997 May 6; revised 1997 December 23

ABSTRACT

We have developed a robust computer program that quickly and efficiently searches for moving objects in large-format CCD images. We describe the initial application of this program to a survey for Kuiper belt objects (KBOs) and Centaurs along the path of NASA's planned Pluto Express mission. Tests have been made to quantify our survey sensitivity, indicating an effective sky area of 2.22 deg^2 searched to a limiting visual plus red "VR" magnitude of 23.1 and an effective area of 0.65 deg^2 searched to a limiting VR magnitude of 23.5. The first data set consists of fields near the expected postrendezvous flight path of the Pluto Express mission, and analysis resulted in the detection of two KBO candidates. The second data set is from a region at higher Galactic latitude, and it produced a further two KBO candidates.

Key words: celestial mechanics, stellar dynamics — planets and satellites: individual (Pluto) — techniques: image processing

1. INTRODUCTION

In NASA's Pluto Express mission, two spacecraft will rendezvous with Pluto near the year 2013. After the encounter, the spacecraft will retain sufficient power and propellant to fly close to a large Kuiper belt object (KBO). The density of KBOs larger than 100 km in diameter near Pluto is on the order of 1 AU^{-3}. It is estimated that the spacecraft velocity must be changed by only $\Delta V \sim 50$–80 m s^{-1} in order to secure a KBO encounter (Lunine et al. 1995, pp. 44, 40–42, 52). Since each spacecraft will be launched with fuel for $\Delta V = 320$ m s^{-1}, it is probable that enough fuel will remain after the Pluto flyby for a KBO encounter. The Pluto Express spacecraft could image the surface of a KBO at visible wavelengths, take infrared and ultraviolet spectra, and perhaps perform radio occultations with Earth. This would help to characterize the KBOs by in situ observation. However, before a KBO flyby can take place, suitable target objects must be identified.

We are conducting a survey to find KBOs near enough to Pluto at the time of the spacecraft flyby for a possible visit. Our survey is sensitive to both KBOs and Centaurs, referred to collectively as slow-moving objects (SMOs). The survey uses the University of Hawaii's 8192 × 8192 (8K) pixel CCD (described in detail below), which images 0.09 deg^2 per field. With this instrument, we maintain a data collection rate so high that computer-based automated object detection is mandatory for real-time analysis. The ability to find objects in real time is very important, because experience has shown that an object discovered on one night will likely be lost if it is not observed again a few nights later and then again in the following month.

Accordingly, we developed a computer program to search the data automatically. Our first specification for the program is that it must be fast. We further require that the program be robust and self-consistent; it should not be overly sensitive to parameters, like seeing, that may vary over the course of a night. In order to implement these two criteria, we thought it best to keep the program as simple as possible by using efficient and stable algorithms as our building blocks.

Since the early 1980s, many attempts have been made to create computer algorithms capable of moving-object detection, using a wide variety of hardware and software setups. Among the earliest are Davies et al. (1984), McMillan et al. (1986), and Taff et al. (1986). Most of these investigations have concentrated on the detection of fast-moving asteroids and have had only rudimentary discussions of algorithm efficiency at object detection. Here we focus on algorithms that have been used to search for objects in the outer solar system.

The Spacewatch project (Gehrels 1991) has been investigating automatic detection algorithms since its inception in 1981. Their algorithm, MODP, uses streak detection to identify fast-moving objects by fitting a set of parameters to each object, in order to distinguish streaked objects from stellar objects. In addition, consistent motion criteria are used to find slower objects by comparing lists of object coordinates in successive images (Jedicke 1995; Rabinowitz 1991). Jedicke & Herron (1997) have computed the efficiency of Spacewatch's real-time algorithm by detecting asteroids with known orbits for a standard set of algorithm parameters. Although they are insensitive to objects with projected velocities less than 6″ hr^{-1}, effectively ruling out most SMOs, their method of evaluating algorithm efficiency is very reliable, as they observe known objects to estimate computer algorithm performance. With an average efficiency of about 65%, Spacewatch has discovered three new Centaurs.

Levison & Duncan (1990) first attempted the search for KBOs in an automated fashion, also using an object-list–based algorithm. They adopt a single parameter to parameterize object shape that does not require iterative fitting, and they reject nonstellar objects based on this quantity. Consistent motion criteria are applied to nonstationary stellar objects to produce a list of candidates. They did not publish the efficiency of their algorithm, and their survey detected no objects.

Irwin, Tremaine, & Żytkow (1995) were the first to detect KBOs with an automated algorithm. Their algorithm deviates from the previous two in that it creates difference maps

TABLE 1

THE 28 PLUTO EXPRESS FIELDS SEARCHED FOR SLOW-MOVING OBJECTS

Field	R.A. (J2000.0)	Decl. (J2000.0)	l	b	UT Date (1996)
PE027	16 43 00	−19 44 23	359 22 51	16 55 59	May 17
PE001[a]	16 43 00	−19 25 22	359 38 31	17 07 41	May 14
PE028	16 44 20	−19 44 22	359 34 56	16 41 09	May 17
PE002	16 44 20	−19 25 22	359 50 37	16 52 47	May 15
PE029	16 45 40	−19 44 20	359 46 59	16 26 17	May 21
PE003[a]	16 45 40	−19 25 21	000 02 40	16 37 52	May 14
PE030	16 47 00	−19 44 21	359 58 56	16 11 21	May 21
PE004	16 47 00	−19 25 22	000 14 38	16 22 54	May 15
PE031	16 48 20	−19 44 23	000 10 48	15 56 23	May 21
PE005	16 48 20	−19 25 22	000 26 33	16 07 54	May 15
PE032	16 49 40	−19 44 23	000 22 39	15 41 23	May 21
PE006	16 49 40	−19 25 22	000 38 24	15 52 52	May 15
PE033	16 51 00	−19 44 23	000 34 26	15 26 22	May 21
PE007	16 51 00	−19 25 22	000 50 12	15 37 48	May 15
PE034	16 52 20	−19 44 23	000 46 09	15 11 19	May 21
PE008	16 52 20	−19 25 23	001 01 56	15 22 42	May 16
PE035	16 53 40	−19 44 20	000 57 51	14 56 16	May 22
PE009	16 53 40	−19 25 22	001 13 37	15 07 35	May 16
PE010	16 55 00	−19 25 22	001 25 14	14 52 25	May 16
PE011	16 56 20	−19 25 21	001 36 49	14 37 15	May 16
PE012[a]	16 57 40	−19 25 22	001 48 18	14 22 00	May 14
PE013	16 59 00	−19 25 22	001 59 45	14 06 45	May 15
PE014[a]	17 00 20	−19 25 22	002 11 09	13 51 28	May 14
PE015	17 01 40	−19 25 22	002 22 29	13 36 10	May 16
PE016	17 03 00	−19 25 22	002 33 46	13 20 49	May 16
PE017	17 04 20	−19 25 22	002 44 59	13 05 27	May 17
PE018	17 05 40	−19 25 22	002 56 10	12 50 03	May 17
PE020[a]	17 08 20	−19 25 22	003 18 21	12 19 09	May 14

[a] Chip 0 malfunctioning, area imaged reduced by $\frac{1}{8}$.

NOTE.—Units of right ascension are hours, minutes, and seconds, and units of declination and Galactic longitude and latitude (l, b) are degrees, arcminutes, and arcseconds.

of adjacent images in the sequence, searching for positive-negative image pairs, indicating a moving object. "Monte Carlo" simulations of artificial moving objects were used to estimate the efficiency of their algorithm at nearly 100% for bright objects, and their survey found two new KBOs.

The primary purpose of this paper is to demonstrate the utility of our recently developed computer program as a tool for finding moving objects in a sequence of images. Of the algorithms reviewed, ours is most similar to the Levison & Duncan (1990) algorithm, as ours is list-based and uses a single quantity to describe object shape. Previous developers of automated software have estimated program efficiency, but there has never been an attempt in the literature to show that an automated algorithm is robust, i.e., the algorithm performance efficiency is insensitive to operating parameters. We believe this paper represents the first time a moving-object detection program has been extensively tested to characterize its performance and prove its robustness. The Pluto Express survey is only one of several solar system surveys in progress with the 8K CCD. It seems worthwhile to describe the operation of this device in some detail.

2. OBSERVATIONS

Observations were taken using the University of Hawaii (UH) 2.2 m telescope on Mauna Kea. The UH 8K pixel mosaic CCD camera was used to obtain the images. This large CCD was developed at the Institute for Astronomy (Luppino et al. 1996). It consists of eight 4096 × 2048 pixel chips tiled to create a 13 cm square detector. These are thick chips, with a resulting high sensitivity to cosmic rays (CRs). On the UH 2.2 m telescope with f/10 focal ratio, the CCD plate scale is $0\farcs35$ pixel^{-1}. A single readout of the 8K array generates 134 Mbyte of raw data, so we used 2 × 2 binning mode for these observations (4 pixels are combined to form 1 image pixel). This saves a factor of 4 in readout time and

TABLE 2

HIGH GALACTIC LATITUDE FIELDS SEARCHED FOR SLOW-MOVING OBJECTS

Field	R.A. (J2000.0)	Decl. (J2000.0)	l	b	UT Date (1996)
HL001	14 01 00	−12 20 00	328 19 19	47 04 49	May 21
HL002	14 02 20	−12 20 00	328 45 40	46 57 07	May 21
HL003	14 03 40	−12 20 01	329 11 51	46 49 17	May 21
HL004	14 05 00	−12 20 00	329 37 56	46 41 22	May 22
HL005	14 06 20	−12 19 58	330 03 51	46 33 20	May 22
HL006	14 07 40	−12 20 00	330 29 37	46 25 08	May 22
HL007	14 09 00	−12 20 00	330 55 15	46 16 50	May 22
HL008	14 10 20	−12 20 00	331 20 43	46 08 25	May 22

NOTE.—Units of right ascension are hours, minutes, and seconds, and units of declination and Galactic longitude and latitude (l, b) are degrees, arcminutes, and arcseconds.

disk space but does not significantly increase confusion between stellar images and CRs.

Seeing for the six survey nights ranged from 0.″7 to 1.″0 FWHM, with an average of 0.″8 FWHM. Three consecutive 800 s exposures were taken of each field, separated by the CCD readout time ($\sim$3 minutes). From experience, three is the optimal number of images for deep SMO surveys. Confusion caused by chance alignments of CRs and/or background noise spikes often occurs with only two images, while four images do not improve the successful identification of SMOs enough to warrant the extra time expended. In order to maximize the camera sensitivity, we used a custom filter (hereafter VR) designed to pass both V- and R-band photons (5000 Å $< \lambda <$ 7000 Å). The CCD quantum efficiency across the VR band averages 0.45. This is about half the quantum efficiency of the coated Tektronix 2048 $\times$ 2048 CCD used in previous Mauna Kea survey work (Jewitt & Luu 1995; Jewitt, Luu, & Chen 1996). However, the reduced efficiency of the 8K CCD is more than offset by its greater total area, resulting in a net improvement in our ability to detect distant objects.

Observations were taken near opposition and divided between 28 "Pluto Express" (PE) fields and eight high Galactic latitude (HL) fields. Typical background object densities are 3×10^5 deg^{-2} for PE fields and 8×10^4 deg^{-2} for HL fields. The PE fields (provided by B. Owen & S. Matousek, JPL) were chosen to fall along the post-encounter trajectory of the Pluto Express spacecraft projected into the plane of the sky. They were corrected for motion in the 1996–2013 interval assuming circular orbits at 35 AU. The result was a search rectangle about 5° $\times$ 1° in angular extent. Lists of the specific fields imaged can be found in Tables 1 and 2. More detailed information on the limiting magnitude and effective sky coverage appears in § 4.

3. THE DETECTION PROGRAM

The program, called Moving Object Detection Software (MODS), was coded in C and C++. An effort was made at all points to create efficient code by reducing the number of steps in any procedure to the minimum necessary. The four discriminants used by Jewitt & Luu (1995) were applied to objects in the image sequence before follow-up observations were made on successive nights. Specifically, we required that an SMO candidate have consistent starlike image shape, consistent flux, constant linear velocity, and velocity within limits expected for the Kuiper Belt population. An outline of the eight steps the program takes while searching for moving objects can be found in Table 3. A more detailed description of each of these steps follows. Program performance tests are reported in § 4.

3.1. *Step 1: Data Flattening*

The data were flattened using dithered images of the twilight sky. Stars in the flat-field images were removed by computing the median of the flat-field image set.

3.2. *Steps 2–4: Object Identification and Characterization*

The program generates a list of all objects in each image frame. This is done by scanning a circular aperture over each flattened image. Any real object must be a local maximum of flux greater than the background defined by the minimum flux threshold ($S_{\min}$),

$$S_{\min} = k\sigma ,$$

where σ is the standard deviation of fluctuations in the sky background for each image and k is a user-selected scaling factor (see § 4). We found that background fluctuations are closely Gaussian, so σ is measured directly from the FWHM of a histogram of pixel counts centered on the background level (step 2). To ensure that each object is recorded only once, it is characterized only when the scanning aperture's center pixel is the local maximum in the aperture. Thus, an object is only counted when the aperture is centered on the object. This method sometimes fails if an object's peak falls between two pixels and those two pixels have the exact same value. In practice, this happens less than 0.5% of the time and does not reduce the possibility that a moving object will be detected.

Each detected object is characterized by its position, flux, and shape (step 3). The positon and associated positional uncertainty are estimated by computing the center of flux (analogous to a center of mass) within the aperture. We find that this location is typically within $\pm$0.25 pixels of centroids computed by more time-consuming Gaussian fits to objects.

The flux is measured by using circular aperture photometry. The local background is estimated by computing the median value in an annulus surrounding the aperture, effectively rejecting CRs. The sky-subtracted aperture intensities are then summed to produce the object flux.

The first of the four criteria for a potential SMO is a shape consistent with the point-spread function (PSF) for the night (step 4). We define the "concentration"

$$C = I_{\max}/\sum I_{ij} ,$$

where $I_{\max}$ is the count in the brightest pixel and the summation yields the total object intensity above background. With this definition, a CR contained within a single pixel would have $C = 1$. Figure 1 shows the distribution of C among the objects in a typical image. The distribution of values for starlike objects is roughly Gaussian, with a mean of 0.084 $\pm$ 0.006. We set liberal limits on the concentration, requiring $C < 0.25$ for potential SMOs. Any objects with $C > 0.25$ are rejected as probable CRs. The computed value of C for an object is a function of the seeing (roughly $\propto \theta^{-2}$, where θ is the seeing) however, the requirement that $C < 0.25$ is generous. Thus, stellar objects are not rejected as CRs, even for the finest seeing in the data set. This CR rejection technique provides a fast and stable alternative to fitting objects with a PSF. By the end of this stage of program operation, a large list characterizing all objects on the image has been generated.

3.3. *Step 5: Image Alignment*

Imperfections in the pointing of the telescope lead to small positional offsets between successive images of a given field. The offset required to align two images of the same field is found using subsets of roughly 65 objects located near the center of each image and selected to be neither CRs, nor overexposed sources, nor background fluctuations. The coordinates in these reduced object lists are shifted until a maximum cross-correlation between objects is found. This determines the offset applied to all object coordinates in the main list. There is minimal focal-plane distortion in our images, so linear shifts are sufficient. We find that the absolute errors in image alignment average 0.″1 for both axes summed in quadrature.

TABLE 3

SEARCH STEPS

Step	Description
1.....	Flatten data
2.....	Determine standard deviation of sky background
3.....	Identify all objects; record flux, position, and concentration
4.....	Reject cosmic rays
5.....	Align images
6.....	Reject stationary objects
7.....	Select velocity; it must be consistent and within limits
8.....	Require consistent flux
9.....	Mark objects and verify by eye

3.4. *Steps 6 and 8: Stationary-Object Rejection and Flux Criterion*

Since stationary objects are of no interest in this survey, we would like to reject them before applying the velocity criterion. If an object is found within the same seeing disk in all three images, it is considered stationary. In addition, the object's flux must not vary between frames by more than a factor of 3. This flux criterion is applied in two places: once during the stationary-object rejection routine to ensure that only nonvarying objects are rejected, and once after the velocity selection criterion to ensure that only nonvarying objects are accepted as candidate SMOs. The flux criterion is chosen to be generous because flux fluctuations from a chance CR falling on an object should not keep it from being classified as a nonvarying object.

3.5. *Step 7: Velocity Criterion*

At this point, the program has a list of all objects that are neither CRs nor stationary objects. A search is now made for constant linear motion at a velocity characteristic of SMOs, the second and third criteria for an SMO candidate. If a path of constant linear velocity can be traced through the images within the $\sim 3\ \sigma$ positional errors, the set of three objects is advanced to the next step. For this work, we selected the apparent opposition speed to be between 2″ and 10″ hr^{-1}, corresponding to heliocentric distances from about 10 to 65 AU, assuming circular Keplerian orbits (Luu & Jewitt 1988). This includes both Centaurs and KBOs but rejects Jovian Trojan asteroids and other near-Earth and main-belt objects (Jewitt & Luu 1995). The rejected group of objects have apparent velocities large enough that it would become necessary to account for trailing loss due to our 800 s integrations (Jewitt et al. 1996). The three exposures cover a time base of about 45 minutes, indicating a minimum displacement of about 0.″8 between images for the slowest objects within our survey's sensitivity.

The final step in the velocity selection is to make sure the apparent motion is retrograde and along the ecliptic. In this survey, candidate SMOs were rejected if their projected sky-plane velocity vectors fell outside a $\pm 30°$ range from moving westward along the ecliptic. This is sufficient to select any object in Keplerian orbit between 10 and 65 AU. In later and continuing surveys with the 8K CCD, we have relaxed the inclination constraint so that any retrograde apparent motion is allowed. Applying the velocity selection criterion yields the final list of candidate SMOs.

3.6. *Step 9: Verification*

The flattened images are marked with the list of candidate SMO positions and displayed in sequence. These marked frames are "speed blinked" by eye, because the eye

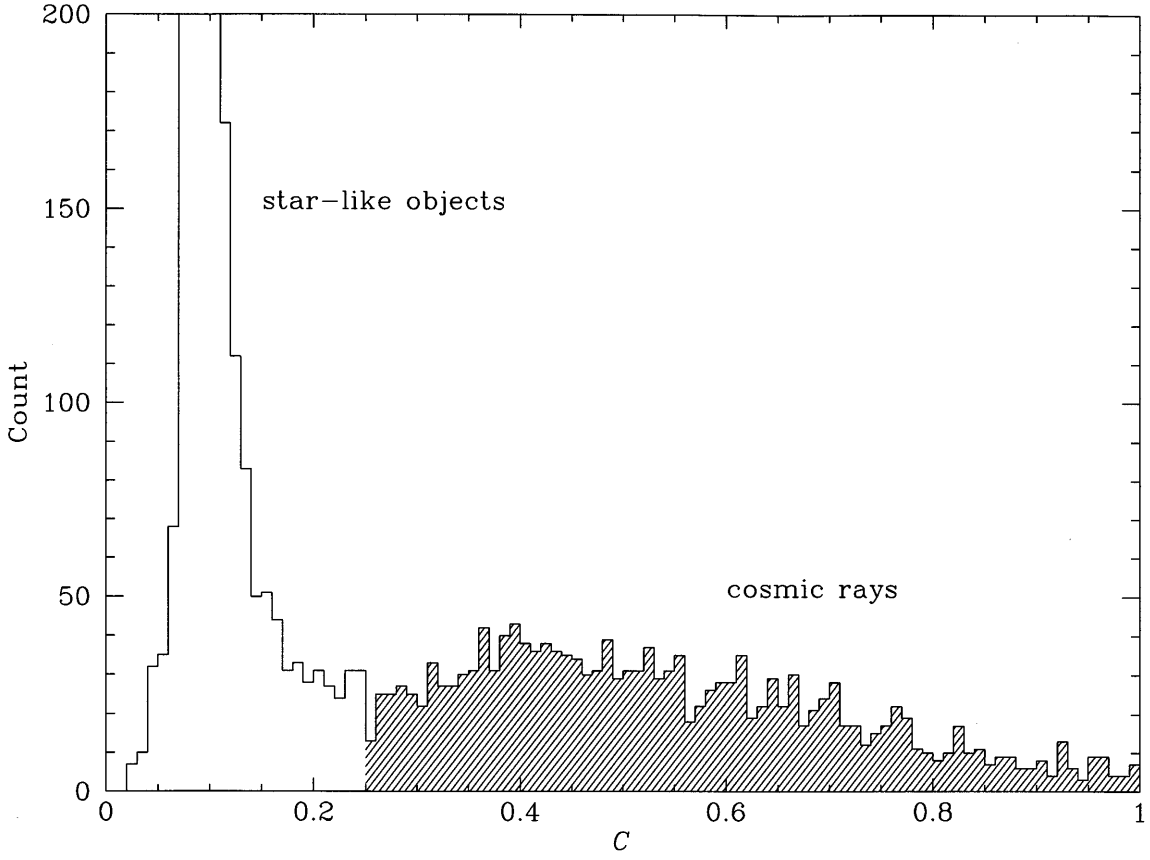

FIG. 1.—Frequency histogram of object concentration C. Objects with $C > 0.25$ (most likely to be cosmic rays) are hatched. The peak of starlike objects extends to a count of 1050.

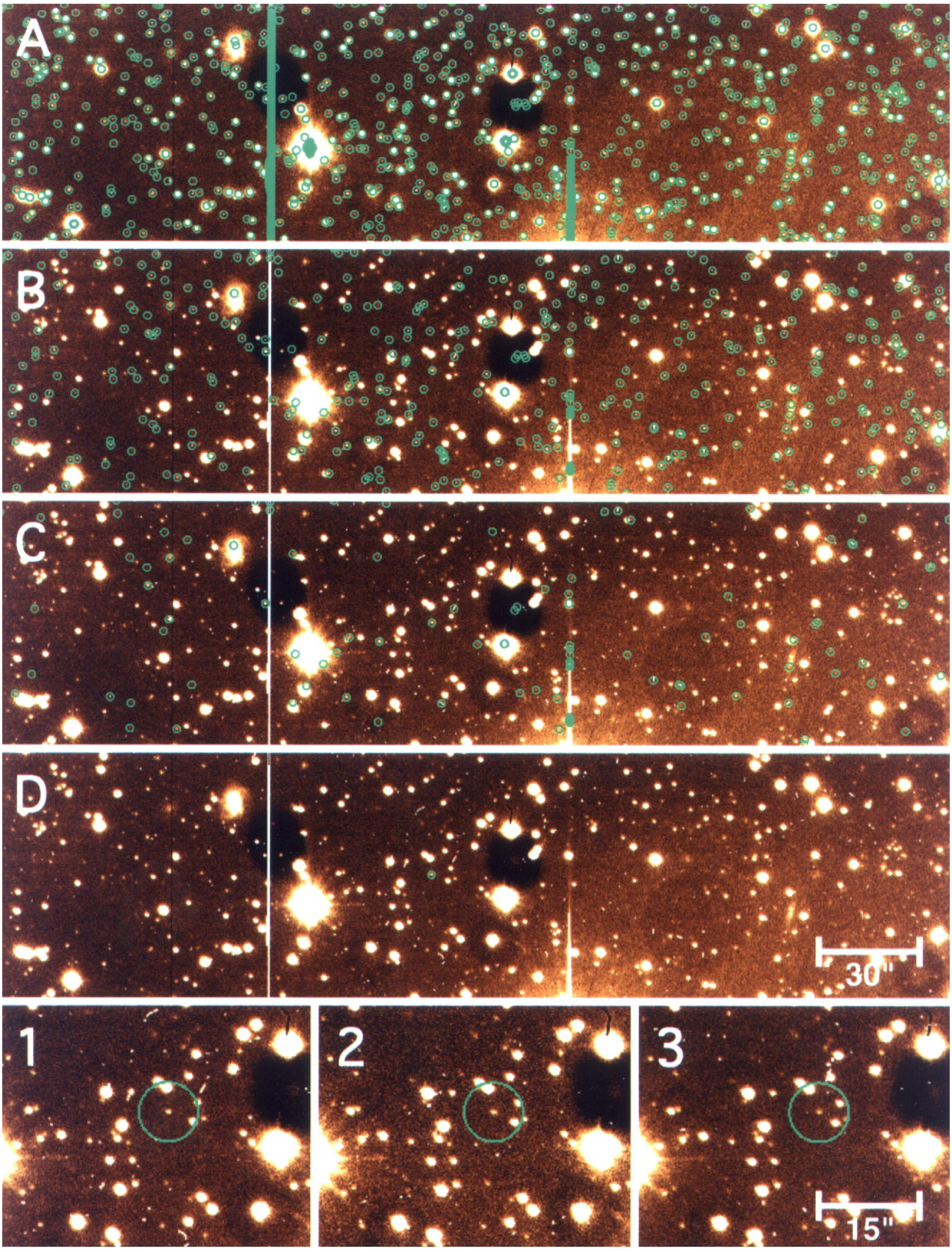

FIG. 2.—Stages of program operation on KV_1 fields. Images A–D are identical sections from the first image in a sequence, accounting for 1.6% of the area of the mosaic. In A, all objects are identified. In B, stationary objects have been rejected. In C, cosmic rays have been rejected, and in D, velocity and consistent flux criteria were applied using the other images in the sequence, leaving only KV_1 marked. Images 1–3 show KV_1's westward movement in the three images. North is up.

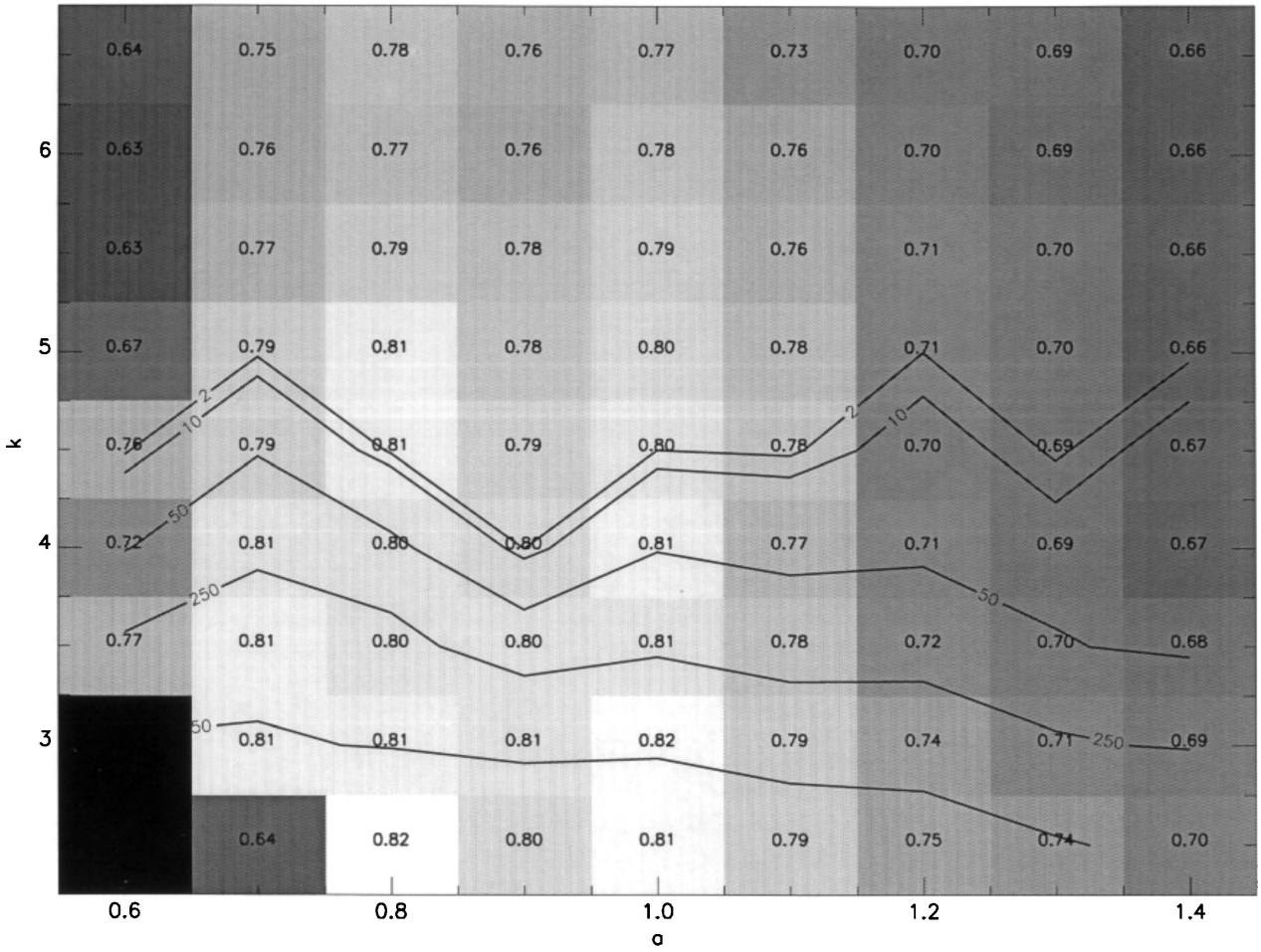

FIG. 3.—Program performance characterized by the two principal parameters, k (in σ above sky noise) and a (in units of actual seeing for the night). The grid brightness and number represent the fraction of correctly identified artificial moving objects (see texts for object distribution). The contours are factor of 5 increases in the number of false detections, beginning with two.

is much better at discerning real candidates than even a very advanced algorithm. An illustration of program operation through the various stages can be found in Figure 2. The images from this figure come from the field in which 1996 KV_1 was found and provide an example of the many obstacles faced by MODS. Two dark spots and several ring-shaped structures can be attributed to shadows of dust specks and internal reflections from a bright source just below the pictured image section, respectively. A diffraction spike near the center of the image can also be seen from this same source. A blocked column (about one-third of the way across the image from the left) and background variation are other undesirable anomalies that can be found in the data. Despite this, we find that spurious detections typically number a few per CCD and most commonly originate from diffraction spikes near overexposed stars or CCD defects. Other sources of confusion include chance alignments of background noise bumps and multipixel CR strikes. At this point, it becomes a simple matter for the researcher to distinguish SMOs from spurious detections, for true SMOs have much more constant velocity vectors and more stable PSFs than spurious detections. By using this technique, blinking time is typically an order of magnitude shorter than unassisted blinking by eye. All potential SMO candidates were imaged on successive nights to further constrain their orbital parameters.

TABLE 4

VR MAGNITUDE OF OBJECTS WITH INSTRUMENTAL FLUX OF 1 COUNT PER SECOND

Chip	m_R
0.....	23.99 ± 0.03[a]
1.....	24.35 ± 0.02
2.....	24.21 ± 0.02
3.....	24.59 ± 0.03
4.....	24.36 ± 0.04
5.....	24.59 ± 0.03[a]
6.....	23.80 ± 0.02[a]
7.....	24.22 ± 0.03[a]

[a] Estimated standard deviation.

4. SENSITIVITY

The most important part of any survey is the determination of its sensitivity. Without this, it becomes impossible to compare results with any other survey. The use of a robust computer program allows us to easily evaluate its performance with simulated data.

4.1. *The Parameter Space*

The user must supply two principal parameters for each survey field: the aperture size for centroiding and photom-

etry, and the aforementioned scaling factor k for the sensitivity of the survey. Since we expect the optimum aperture size to be proportional to the seeing for the night, we define

$$R = a\theta ,$$

where R (arcseconds) is the radius of the aperture, θ (arcseconds) is the seeing (median FWHM of nonsaturated stellar objects), and a is the dimensionless aperture scaling factor. If a is overestimated, two nearby stars may be counted as only one object by the program. An underestimate leads to the possibility of one object being "split" into two if it has a lumpy morphology. The optimum k-value is also constrained; if k is too high, detectable SMOs may be missed, while a low k will produce many false detections from sky noise. We seek to evaluate program performance for a range of principal parameter values to find the optimum operational values.

A typical star field imaged on one CCD of the mosaic was chosen for this program performance evaluation. Artificial SMOs were generated using a long-period multiplicative congruential random-number generator (Press et al. 1992, p. 282), uniformly spaced in speed, projected inclination, magnitude, and position for ranges described below. The two principal parameters were then varied, and a count of the number of correctly identified objects and false detections was made. The results of this test are presented in Figure 3. Note that the grid values represent the fraction of total simulated objects successfully detected, many of which were faint. Since we seek to minimize false detections and maximize real detections, the area of ideal operation corresponds to $4.5 \leq k \leq 5$ and $0.8 \leq a \leq 1.0$. Note that, in this area, the number of successful detections is insensitive to the principal parameters, while the logarithm of the number of false detections is approximately inversely proportional to k. For this survey, we chose $k = 5$ (threshold equal to 5 σ above sky) and $a = 1.0$ (aperture radius equal to the FWHM of the seeing disk).

4.2. *Limiting Magnitude Determination and Effective Sky Coverage*

Photometric measurements were made to determine the sensitivity of each of the CCDs using Landolt (1983, 1992) standard stars. Landolt's V and R magnitudes were converted into magnitudes corresponding to our VR custom filter ($m_{\rm VR}$) by defining $m_{\rm VR} = 0$ as the flux received through the VR filter from a star with both visual magnitude (m_V) equal to zero and red magnitude (m_R) equal to zero. Table 4 shows the $m_{\rm VR}$ of a star imparting 1 count s^{-1} instrumental flux onto each CCD. These values were used to calibrate the flux of artificial moving objects placed on the test images.

The same random-number generator as mentioned above was used to create a set of 2000 artificial SMOs evenly distributed in speed, projected inclination, magnitude, and position for each of the eight mosaic chips. The speed ranges produced were 2″–10″ hr^{-1} and the inclination ranged from $+30°$ to $-30°$ from the ecliptic, corresponding to our selections for the real SMO data search. By running these "Monte Carlo" simulations in batches of 100, the probability of more than one pair of artificial SMOs overlapping per image becomes less than 0.3%. The KBOs were given PSFs matched to real stars with added photon noise. The program was run, and correct identifications were recorded. There was no observed object inclination or speed bias affecting program performance. We used these data to estimate the limiting magnitude and effective sky coverage of our survey.

5. RESULTS

Using the techniques described in § 4, we have plotted the net efficiency of the mosaic, the maximum detection efficiency ($e_{\rm max}$), and the magnitude at which detection efficiency drops to $0.5e_{\rm max}$ ($m_{\rm VR50}$) for the Galalactic latitude bounds of fields imaged in our survey in Figure 4. We use $m_{\rm VR50}$ as our sensitivity limit. Note that this quantity is reduced at low Galactic latitudes because of high background star density. Table 5 gives $e_{\rm max}$ and $m_{\rm VR50}$ for each of the chips and for the CCD as a whole. Note that the even-numbered chips have lower $e_{\rm max}$, because a section of each of these chips was vignetted by the circular VR filter. To compute effective area ($A_{\rm eff}$) from the actual sky area imaged ($A_{\rm act}$), we assert that $e_{\rm max}$ is dominated by a reduction in the CCD area where SMOs may be found. This statement is supported by two observations: (1) the vignetted CCDs have $e_{\rm max}$ roughly inversely proportional to the obscured area, and (2) $e_{\rm max}$ is insensitive to background star density. Thus we obtain the effective area from the formula

$$A_{\rm eff} = A_{\rm act}\, e_{\rm max} .$$

The maximum detection efficiencies are 0.87 for the PE fields and 0.89 for the HL fields. Combining the maximum efficiencies with the true areas surveyed (2.58 deg^2 for PE fields and 0.76 deg^2 for HL fields) yields $A_{\rm eff} = 2.22$ deg^2 of PE fields to $m_{\rm VR50} = 23.1$ and $A_{\rm eff} = 0.65$ deg^2 of HL fields

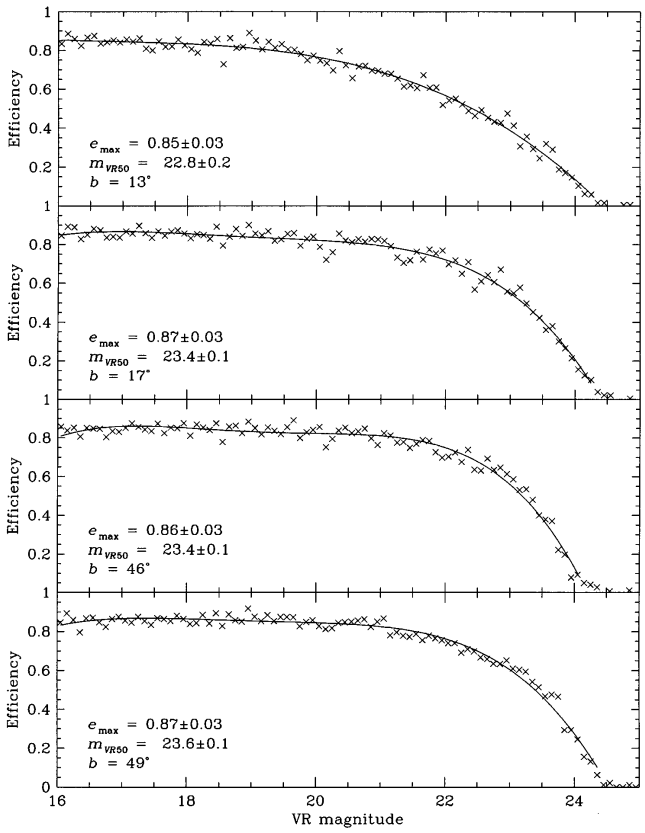

FIG. 4.—Simulated efficiency curves for boundary Galactic latitude fields in the HL and PE searches, combined for all eight chips of the mosaic. A fourth-degree polynomial fit has been overplotted to estimate efficiency quantities; $e_{\rm max}$ is maximum detection efficiency, and $m_{\rm VR50}$ is the magnitude at which detection efficiency drops to $0.5e_{\rm max}$.

TABLE 5

SIMULATED EFFICIENCY CHARACTERISTICS

Field	All Chips	Chip 0	Chip 1	Chip 2	Chip 3	Chip 4	Chip 5	Chip 6	Chip 7
PE018, $b = 12°50'$:									
e_{max}	0.85 ± 0.03	0.86 ± 0.06	0.92 ± 0.06	0.77 ± 0.05	0.86 ± 0.05	0.78 ± 0.07	0.89 ± 0.07	0.87 ± 0.06	0.92 ± 0.06
m_{VR50}	22.8 ± 0.2	22.7 ± 0.3	22.8 ± 0.4	22.9 ± 0.3	23.1 ± 0.2	22.7 ± 0.3	22.8 ± 0.3	22.5 ± 0.3	22.9 ± 0.3
PE027, $b = 16°56'$:									
e_{max}	0.87 ± 0.03	0.93 ± 0.07	0.96 ± 0.05	0.72 ± 0.07	0.87 ± 0.05	0.77 ± 0.07	0.91 ± 0.05	0.92 ± 0.06	0.96 ± 0.07
m_{VR50}	23.4 ± 0.1	23.6 ± 0.2	23.7 ± 0.2	23.7 ± 0.3	23.6 ± 0.1	23.2 ± 0.2	23.2 ± 0.1	23.2 ± 0.2	23.1 ± 0.1
HL008, $b = 46°08'$:									
e_{max}	0.86 ± 0.03	0.86 ± 0.07	0.90 ± 0.06	0.81 ± 0.06	0.89 ± 0.05	0.84 ± 0.06	0.88 ± 0.06	0.84 ± 0.06	0.95 ± 0.06
m_{VR50}	23.4 ± 0.1	23.5 ± 0.3	23.8 ± 0.2	23.3 ± 0.1	23.5 ± 0.1	23.0 ± 0.2	23.3 ± 0.1	23.1 ± 0.2	23.5 ± 0.1
HL000, $b = 49°11'$:									
e_{max}	0.87 ± 0.03	0.88 ± 0.05	0.96 ± 0.05	0.77 ± 0.05	0.90 ± 0.06	0.75 ± 0.08	0.91 ± 0.05	0.88 ± 0.06	0.95 ± 0.04
m_{VR50}	23.6 ± 0.1	23.8 ± 0.2	23.9 ± 0.1	23.9 ± 0.1	23.7 ± 0.1	23.0 ± 0.2	23.5 ± 0.1	23.4 ± 0.3	23.7 ± 0.1

NOTES.—Simulated characteristics for individual chips on the CCD, for boundary Galactic latitude (b) fields in the HL and PE searches. Note that chips 0, 2, 4, and 6 were all partially vignetted by the circular filter, resulting in reduced maximum efficiencies.

to $m_{VR50} = 23.5$. For a simple illustration of typical object sizes, an object 30 AU from the Sun at opposition with albedo 0.04 and diameter 140 km is expected to have an $m_R = 23.0$, which corresponds to $m_{VR} = 23.0$ for a gray body.

This survey resulted in the detection of two KBOs from the PE fields and two KBOs from the HL fields. The implied sky-plane surface density of Pluto Express objects is ~ 0.9 deg^{-2} to $m_{VR50} = 23.1$. This may be compared with a surface density of ~ 1 deg^{-2} (Jewitt et al. 1996) to a corresponding $m_R = 23.1$ for gray objects. The agreement between these numbers suggests that future surveys will locate objects suitable for rendezvous with the Pluto Express spacecraft. Unfortunately, we were only able to recover one of the four detected objects, 1996 KV_1, from the PE fields. This KBO will be reobserved at successive oppositions to more accurately determine its orbital elements. A summary of the orbital information for all objects appears in Table 6 from Marsden (1996a, 1996b).

6. SUMMARY

We have demonstrated that MODS is a useful utility for moving-object surveys. It is both robust and self-consistent, as our studies of the parameter space indicate. The use of a computer program allows the quantification of our survey sensitivity to an accuracy that is infeasible with traditional blinking by eye. In addition, we have applied MODS to a data set that may contain slow-moving objects with which the Pluto Express spacecraft can rendezvous. We have found two near-Pluto KBOs and two KBOs at higher Galactic latitudes. Future surveys will make use of the program to analyze much larger data sets than were conceivable without automated moving-object identification methods.

We thank telescope operators John Dvorak and Chris Stewart for help at the telescope. We thank Steve Matousek and Bill Owen of JPL for providing the PE fields. This research was funded by a grant to D. J. from NASA's Planetary Astronomy Program.

TABLE 6

ORBITAL PARAMETERS OF FOUND KBOS

Name	a (AU)	e	i (deg)	M (deg)	Periastron (deg)	Node (deg)	Arc Length (days)	Epoch (1996)
1996 KV_1[a]	42.966	0.041	8.4	0.12	161.5	91.8	87	Jun 26
1996 KW_1[b]	46.602	0	5.5	0	176.3	38.4	2	May 17
1996 KX_1[b]	39.543	0.097	1.5	359.98	17.9	197.5	2	May 17
1996 KY_1[b]	39.517	0.096	30.9	0	6.0	248.6	8	May 17

[a] Orbital elements from Marsden 1996b.
[b] Orbital elements from Marsden 1996a. Short arc length; parameter values suspect.

REFERENCES

Davies, J. K., Green, S. F., Stewart, B. C., Meadows, A. J., & Aumann, H. H. 1984, Nature, 309, 315
Gehrels, T. 1991, Space Sci. Rev., 58, 347
Irwin, M., Tremaine, S., & Żytkow, A. N. 1995, AJ, 110, 3082
Jedicke, R. 1995, in IAU Symp. 167, New Developments in Array Technology and Applications, ed. A. G. D. Philip, K. A. Janes, & A. R. Upgren (Dordrecht: Kluwer), 157
Jedicke, R., & Herron, J. D. 1997, Icarus, 127, 494
Jewitt, D. C., & Luu, J. X. 1995, AJ, 109, 1867
Jewitt, D. C., Luu, J. X., & Chen, J. 1996, AJ, 112, 1225
Landolt, A. U. 1983, AJ, 88, 439
———. 1992, AJ, 104, 340
Levison, H. F., & Duncan, M. J. 1990, AJ, 100, 1669
Lunine, J. I., et al. 1995, Pluto Express: Report of the Science Definition Team (ed. 1.0; Washington: NASA)
Luppino, G., G., Metzger, M., Kaiser, N., Clowe, D., Gioia, I., & Miyazaki, S. 1996, in ASP Conf. Ser. 88, Clusters, Lensing, and the Future of the Universe, ed. V. Trimble & A. Reisenegger (San Francisco: ASP), 229
Luu, J. X., & Jewitt, D. C. 1988, AJ, 95, 1256
Marsden, B. G. 1996a, Minor Planet Circ., No. 27429
———. 1996b, Minor Planet Circ., No. 27883
McMillan, R. S., Scotti, J. V., Frecker, J. E., Gehrels, T., & Perry, M. L. 1986, Proc. SPIE, 621, 141
Press, W. H., Teukolsky, S. A., Vetterling, W. T., & Flannery, B. P. 1992, in Numerical Recipes in C (Cambridge: Cambridge Univ. Press)
Rabinowitz, D. L. 1991, AJ, 101, 1518
Taff, L. G., Yakutis, A. J., Haase, R. L., & Jonuskis, D. M. 1986, Proc. SPIE, 621, 155